Gate-controlled phase switching in a parametron

Ž. Nosan, P. Märki, N. Hauff, C. Knaut, and A. Eichler*
Laboratory for Solid State Physics, ETH Zürich, CH-8093 Zürich, Switzerland

(Received 23 January 2019; published 6 June 2019)

The parametron, a resonator-based logic device, is a promising physical platform for emerging computational paradigms. When the parametron is subject to both parametric pumping and external driving, complex phenomena arise that can be harvested for applications. In this paper, we experimentally demonstrate deterministic phase switching of a parametron by applying frequency tuning pulses. To our surprise, we find different regimes of phase switching due to the interplay between a parametric pump and an external drive. We provide full modeling of our device with numerical simulations and find excellent agreement between model and measurements. Our result opens up new possibilities for fast and robust logic operations within large-scale parametron architectures.

DOI: 10.1103/PhysRevE.99.062205

I. INTRODUCTION

Many fascinating and useful phenomena arise when the spring constant of a resonator is varied periodically in time. "Degenerate parametric pumping" refers to the important case when the modulation rate is close to twice the natural frequency of the resonator, $f_p \sim 2f_0$ [1]. As long as the modulation depth λ is below a threshold value λ_{th}, parametric pumping simply decreases or increases the effective damping of the resonator in response to external forcing. This effect is used with great success for quantum-limited signal amplification with superconducting Josephson circuits [2–6], feedback damping of nanomechanical resonators and trapped particles [7–9], and squeezing of the vacuum noise of laser light [10–13].

When the modulation depth exceeds the threshold, $\lambda > \lambda_{\mathrm{th}}$, the effective damping drops below zero. The system then becomes a parametric phase-locked oscillator, or "parametron," that undergoes large oscillations at $f_p/2$ even in the absence of external forcing [1,14–16]. Due to the periodicity doubling between pump and oscillation, the parametron features two "phase states" that have equal amplitude but differ in phase by π. In a classical system, the parametron selects one out of the two phases states during a spontaneous time-translation symmetry-breaking event, while a quantum system can reside in a superposition of both states. This state duality has been applied to classical computing before the invention of the transistor [17] and has recently been rediscovered in the context of alternative computational architectures such as neural networks, adiabatic quantum computing and quantum annealing [18–21]. There, the two phase states can represent opposite values of a single variable, e.g., the polarization states of a single spin ("up and down"). An ensemble of parametrons is envisioned as a simulator to find the ground state of Ising Hamiltonians comprising many spins, or equivalent combinatorial optimization problems from other fields. These problems are NP-hard and thus very challenging to solve on conventional computers. Several exciting physical implementations are currently competing to demonstrate such novel computing paradigms, including optical parametric oscillators, superconducting Josephson circuits, and nanomechanical resonators [22–24].

The symmetry between the two phase states can be broken by applying a force at the oscillation frequency $f_p/2 \sim f_0$ [Fig. 1(a)] [25–28]. Depending on the relative phase θ of this force, the parametron will favor one of the states, which can be used for various detection and amplification schemes [16,29–31]. The symmetry breaking has also been found to qualitatively change the bifurcation topology of the parametron, i.e., the way stable and unstable solutions merge and annihilate as a function of f_p [28]. This has surprising consequences for the hysteresis observed when sweeping the pump (at f_p) and the force (at $f_p/2$) simultaneously. In a certain frequency range, the two drives can partially cancel each other, leading to a decrease in amplitude of one parametric phase state and to an additional jump. One of the applications predicted in Ref. [28] is that the parametron can be switched from one phase state to the other simply by changing the resonance frequency f_0 relative to $f_p/2$ with a gate voltage. The "gate parametron" is effectively a new device with a suite of useful properties.

In this paper, we experimentally demonstrate gate-controlled switching of the phase states of a parametron. With an electrical resonator circuit, we first establish the existence of a double hysteresis due to parametric symmetry breaking, which previously has been found in mechanical resonators at much lower frequencies [28,31]. We then proceed to demonstrate phase switching with high fidelity and in close agreement with numerical simulations. The achievable switching rate is ultimately limited by the ringdown time $\tau = \frac{Q}{\pi f_0}$ of the resonator (where Q is the quality factor). We find that the switching works down to a timescale of 7τ, where the dynamics is much too fast for the gate parametron to follow its steady-state response. We believe that the surprisingly fast phase switching stems from the interplay between parametric pumping and external forcing.

*eichlera@ethz.ch

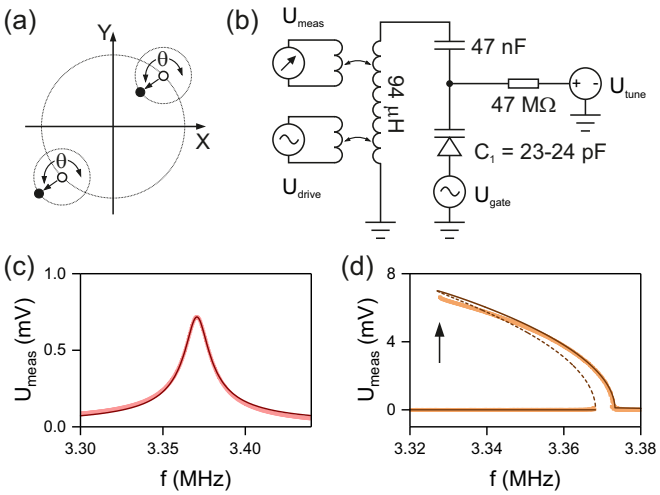

FIG. 1. (a) Phase states of a parametron in the rotating frame (open dots). In-phase amplitude is denoted by X, out-of-phase amplitude by Y. A resonant force with relative phase θ can break the symmetry of the parametron and shift the states (solid dots). (b) In our experiment, an electrical resonator is driven and measured inductively. The varactor diode with capacitance C_1 is biased with U_{tune} and U_{gate} for dc and ac tuning of f_0, respectively. (c) Response to external driving with $U_d = 50\,\text{mV}$ ($U_p = 0$) and (d) parametric response to $U_p = 5\,\text{V}$ ($U_d = 0$) with $U_{\text{tune}} = 2.2\,\text{V}$. Bright dots represent data, fits are shown as lines. The dashed line in panel (d) indicates an unstable solution branch. From the fits, we obtain $f_0 = 3.37\,\text{MHz}$, $Q = 243$, $F_d/U_d = 2.65 \times 10^{10}\,\text{s}^{-2}$, $\alpha = 3.2 \times 10^{17}\,\text{V}^{-2}\,\text{s}^{-2}$, and $\eta = 5.8 \times 10^{8}\,\text{V}^{-2}\,\text{s}^{-1}$.

II. EXPERIMENTAL SETUP

We perform experiments with an electrical circuit whose main elements are a coil and a varactor diode with capacitance C_1 [Fig. 1(b)]. The precise value of C_1 depends on the applied voltage, giving rise to a nonlinearity (see Appendix B for details and calibration). We use a dc voltage U_{tune} to ensure that the diode is in reverse bias, while rapid changes of the resonance frequency $\omega_0 = 2\pi f_0 \approx \sqrt{1/LC_1}$ are induced through U_{gate}. The latter is applied via an operational amplifier (THS4271D) with a nominal unity gain. The low output impedance of this voltage buffer is necessary to preserve the quality factor of the resonator. The resonator is driven and read out inductively with a lock-in amplifier (Zurich Instruments HF2LI).

The equation of motion that governs our system is

$$\ddot{x} + \omega_0^2[1 - \lambda\cos(\omega_p t)]x + \Gamma\dot{x} + \alpha x^3 + \eta x^2\dot{x} = F_d\cos(\omega_d t + \theta), \tag{1}$$

where dots denote differentiation with respect to time t, x is an oscillating voltage, and $\Gamma = \omega_0/Q$ is the damping rate. The varactor diode gives rise to an approximately linear dependence of the spring constant on x. Driving the resonator with a voltage amplitude U_p at a rate $f_p = \omega_p/2\pi$ leads to off-resonant oscillations in the circuit that modulate ω_0^2. In Eq. (1) this parametric effect is accounted for by the second term in square brackets with modulation depth $\lambda \propto U_p$. The nonlinearity is also responsible for the Duffing coefficient α and for the nonlinear damping coefficient η. The resonator can be driven externally with a near-resonant frequency $f_d = \omega_d/2\pi$, an effective amplitude $F_d \propto U_d$, and relative phase θ. For simplicity, we set $x = U_{\text{meas}}$, that is, we treat the voltage in our pick-up coil as the effective resonator displacement. The only modification we incur through this step is that the values of α and η will be normalized accordingly (see Appendix A for all details).

III. MEASUREMENTS

Under a small external drive and for $\lambda = 0$, the resonator oscillates at f_d with an amplitude that is proportional to U_d. From a sweep of the driving frequency, we obtain a Lorentzian response curve that we can use to determine f_0, Q, as well as to calibrate F_d/U_d [Fig. 1(c)]. In the opposite case of purely parametric pumping and $U_d = 0$, a finite response is measured within a certain frequency range when $U_p \geqslant U_{\text{th}}$ [Fig. 1(d)], which allows us to calculate the modulation depth as

$$\lambda = \frac{U_p\lambda_{\text{th}}}{U_{\text{th}}} = \frac{U_p}{U_{\text{th}}}\frac{2}{Q}. \tag{2}$$

Beyond λ_{th}, the device is linearly unstable and enters the nonlinear parametron regime. From a fit to the nonlinear amplitude response, we can extract values for α and η. Here, the nonlinear damping coefficient η is used to model the frequency at which the large-amplitude branch is terminated [see arrow in Fig. 1(d)].

When parametric pumping and external driving are present simultaneously, parametric symmetry breaking occurs [28]. With $f_p = 2f_d$, this can lead to a complex bifurcation topology and a characteristic double hysteresis in frequency sweeps [Figs. 2(a) and 2(b)]. Importantly, the external drive causes the parametron to occupy opposite phase states when sweeping the frequency upwards or downwards.

The mechanism that underlies phase switching is surprisingly simple. Far from resonance, the resonator is outside the region of parametric instability, and no parametric oscillation takes place. The phase of the resonator is then determined by the external drive alone. Due to the phase difference of the driven harmonic resonator below and above resonance, the external drive imprints opposite phases into the system for the two extreme gate voltages. When the detuning is reduced, the resonator enters the region of parametric instability (either from below or above in frequency) and must ring up to one of the two phase states. In this moment, the phase imprinted upon the parametron by the external drive acts as a bias that deterministically selects one of the two phase states. It was proposed that instead of sweeping $f_{d,p}$, one could vary f_0 over time to induce phase state switches [28]. We present an experimental demonstration of this prediction.

We can change f_0 as a function of time by applying a time-varying gate voltage $U_{\text{gate}} = U_{\text{mod}}\cos(2\pi t/T_{\text{mod}})$. In Fig. 2(c) we observe the quasistatic response of the resonator to a modulation of U_{gate} within a period $T_{\text{mod}} \gg \tau = 23\,\mu\text{s}$. The resonator changes indeed between the two phase states once every $T_{\text{mod}}/2$, confirming the possibility of gate-controlled phase switching.

We have tested periodic phase switching with varying speed and found two distinct regimes. In Figs. 3(a) and 3(b) the voltage U_{gate} is modulated slowly. Both amplitude and phase follow the response expected from quasistatic

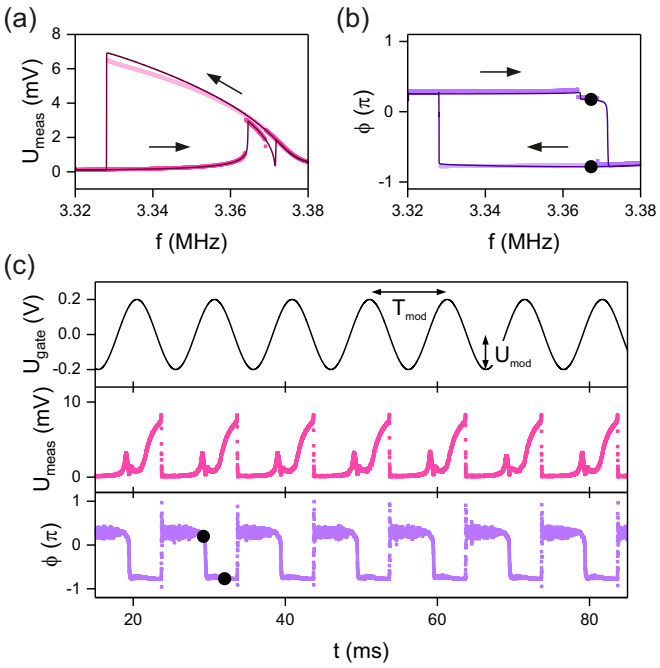

FIG. 2. (a) Amplitude and (b) phase response during sweeps of f with parametric pumping (at $f_p = 2f$) and external driving (at $f_d = f$) applied simultaneously. A characteristic double hysteresis is observed, with two jumps when sweeping from low to high frequency and one jump in the opposite direction. In all graphs, bright squares are measurements and dark lines are simulations. Black dots in panel (b) indicate the position of the phase states in frequency. $U_{\text{tune}} = 2.2\,\text{V}$, $U_{\text{gate}} = 0$, $U_p = 5\,\text{V}$, $U_d = 50\,\text{mV}$, $\theta = \pi/4$. (c) Response to a periodic voltage U_{gate} that shifts f_0 relative to the fixed $f_{p,d}$. Black dots indicate the approximate positions of the two phase states within one U_{gate} period. $f_p = 2f_d = 6.74\,\text{MHz}$, $U_{\text{mod}} = 0.2\,\text{V}$, and $T_{\text{mod}} = 10\,\text{ms}$.

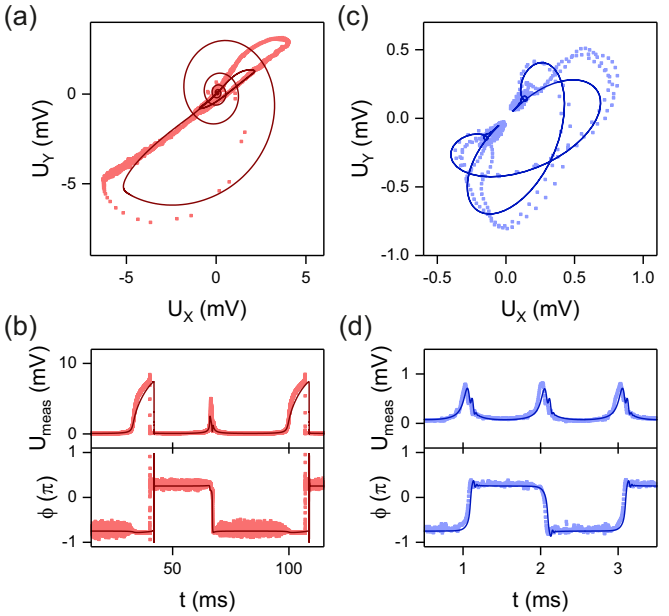

FIG. 3. Periodic response of the parametron to U_{gate} modulations (a) in the rotating frame of the lock-in amplifer (i.e., the in-phase and out-of-phase quadratures U_X and U_Y at $f_p/2$) and (b) in terms of amplitude and phase as a function of time. Bright squares are measurements, solid lines are simulations. The starting phase of the gate voltage modulation is a free parameter in the simulation. $U_{\text{tune}} = 2.2\,\text{V}$, $U_p = 5\,\text{V}$, $U_d = 50\,\text{mV}$, $\theta = \pi/4$, $T_{\text{mod}} = 67\,\text{ms}$, and the pulse has an amplitude of $U_{\text{mod}} = 0.45\,\text{V}$. In panels (c) and (d) we show the same for $T_{\text{mod}} = 2\,\text{ms}$.

frequency sweeps [cf. Fig. 2(a) and 2(b)], and the phase space picture in Fig. 3(a) is asymmetric. Upon decreasing the modulation period, we reach a qualitatively different behavior. In Figs. 3(c) and 3(d), the amplitude remains much smaller and the phase space picture is almost symmetric, i.e., the gate parametron does not follow its steady-state solution. Surprisingly, the resonator still undergoes phase switches. Numerical Runge-Kutta simulations reproduce all of the observed features (see Appendix C for details).

Gate-induced phase switches rely on the formation of a hysteresis. To gain a deeper insight into the different regimes observed in Fig. 3, we have investigated the hysteresis of the gate parametron as a function of T_{mod} in Fig. 4(a). The large hysteresis observed for slow modulation ($T_{\text{mod}} = 67\,\text{ms}$, bottom trace) breaks down and reaches a minimum width at $T_{\text{mod}} \sim 12.5\,\text{ms}$. From there, the hysteresis is found to monotonically increase down to the shortest T_{mod}, albeit with a more symmetric shape than for slow modulations. Numerical simulations confirm the experimental results.

We believe that the hysteresis for short T_{mod} is dominated by the behavior of the underlying harmonic oscillator. If the driving frequency of any resonator is ramped fast enough, the response follows with a delay and a hysteresis develops even in the absence of nonlinearities. In Fig. 4(b) we have measured the resonator response without parametric pumping. Indeed, we observe that a hysteresis arises for short T_{mod} that resembles the one in Fig. 4(a).

IV. DISCUSSION

We conclude that the two regimes of phase switching arise due to the interplay between the parametric pump and the external drive. For slow evolutions, the resonator follows the amplitude and phase dictated by the parametric pump, and the external drive merely acts as a symmetry breaking force. The parametron can directly switch between the slightly asymmetric phase states. For rapid evolutions, it is the external force that dominates the response, and the only visible influence of the parametric drive is a broadening of the hysteresis [compare the upper traces in Figs. 4(a) and 4(b)]. After the phase flip, the parametron relaxes into the appropriate phase state. Gate-controlled phase state switching is thus still possible in this regime.

As a summary, we have demonstrated the main functionality of the gate parametron, namely, deterministic and gate-controlled phase state switching due to a symmetry-breaking force. More generally, we observed phase switching of the gate parametron on timescales down to $T_{\text{mod}}/2 = 7\tau$ for a single switch, and we found two distinct regimes of hysteresis formation due to the interplay between the parametric pump and the external drive. Our gate-controlled phase-switching technique allows individual control of any number of parametrons sharing one parametric drive at f_p and one external drive at $f_p/2$. It thus offers a simplified architecture for large-scale implementations of parametrons, which may

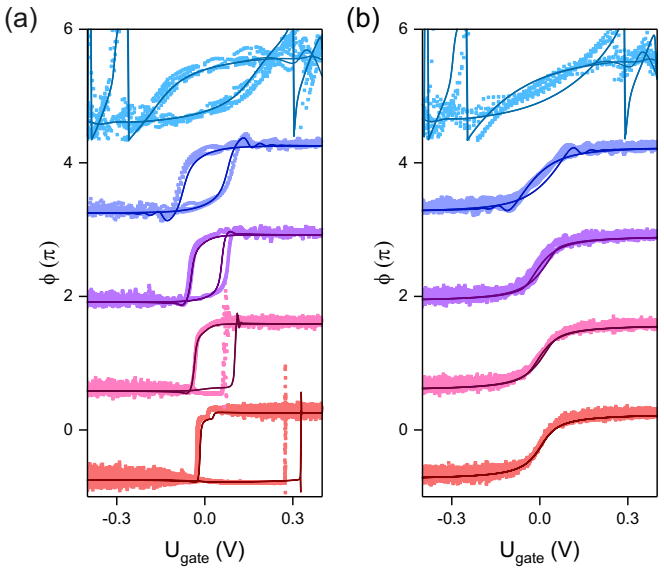

FIG. 4. Hysteresis in the phase response to U_{gate} modulations. Bright squares are measurements, solid lines are simulations, and curves are offset for visibility. (a) Response for $T_{\text{mod}} = 67$ ms, 12.5 ms, 6.7 ms, 2 ms, and 0.33 ms from bottom to top, with $U_{\text{tune}} = 2.2$ V, $U_p = 5$ V, $U_d = 50$ mV, $U_{\text{mod}} = 0.45$ V, and $\theta = \pi/4$. (b) The same study for $U_p = 0$. Note that the color coding for T_{mod} is consistent with Fig. 3.

be crucial for novel computation paradigms such as neural networks, adiabatic quantum computing, and quantum annealing [18–21].

Ongoing and future work will address additional features of the gate parametron. For instance, logic gate operations, such as originally proposed by Goto [17], should be straightforward to implement with the gate parametron (see Appendix D). We suggest that performing logic operations with a gate voltage instead of a clocked sequence of parametric drives [17] allows for more versatile logic architectures. For quantum systems, it will be interesting to study the possibility of rapid generation of quantum superpositions between the phase states of a gate parametron [see Ref. [32] or the steady-state transition in Fig. 1(c) of Ref. [33]] and of entanglement between coupled parametron devices. All of these applications may be implemented in a variety of resonators, ranging from optical parametric oscillators to Josephson junction circuits, nanomechanical resonators, and levitating particles [9,22–24].

ACKNOWLEDGMENTS

The authors acknowledge fruitful discussions with O. Zilberberg, R. Chitra, and T. Heugel. This work received financial support from the Swiss National Science Foundation (CRSII5_177198/1) and from a Public Scholarship of the Development, Disability and Maintenance Fund of the Republic of Slovenia (11010-247/2017-12).

APPENDIX A: DERIVATION OF THE EQUATION OF MOTION

In order to obtain the equation of motion for our resonator, we use Kirchhoff's second law and express the equation in terms of charge q as

$$\ddot{q} + \omega_0^2 q + \Gamma\dot{q} + \tilde{\beta}q^2 + \tilde{\eta}q^2\dot{q} = \frac{U_1}{L}\cos(\omega t + \theta) + \frac{U_2}{L}\cos(2\omega t + \phi). \tag{A1}$$

Here L is the inductance of the circuit, $U_{1,2}$ are forcing terms, and $\tilde{\beta}$ is the coefficient of an antisymmetric potential contribution, i.e., it reflects the fact that ω_0^2 is approximately linearly dependent on the applied voltage (charge) due to the varactor diode. The nonlinear damping term with coefficient $\tilde{\eta}$ is needed to model the termination of the large-amplitude branch of the parametron. In this system, nonlinear damping corresponds to a loss of charge when large voltage oscillations overcome the reverse bias and the silicon varactor diode has a finite resistance for a short time during the oscillation period.

We can transform Eq. (A1) using the fact that the quadratic nonlinear term can be expressed as an effective cubic term $\tilde{\alpha}x^3$ [1]. Furthermore, the forcing due to U_2 will generate modulations of the potential that we take into account in the form of a parametric pump with modulation depth λ (think of $\tilde{\beta}q$ as a time-dependent potential contribution). The equation then becomes

$$\ddot{q} + \omega_0^2[1 - \lambda\cos(2\omega t + \phi)]q + \Gamma\dot{q} + \tilde{\alpha}q^3 + \tilde{\eta}q^2\dot{q} = \frac{U_1}{L}\cos(\omega t + \theta), \tag{A2}$$

where $\tilde{\alpha}$ is the coefficient of a Duffing nonlinearity.

It is convenient to treat the system in terms of the voltages that we measure and apply by the two secondary coils, which are inductively coupled to the main circuit. Therefore we introduce two proportionality factors n_1 and n_2, where the first describes a relation between charge and measured voltage, $x = U_{\text{meas}} = n_1 q$, while the other defines a relation between the applied and induced voltages, $U_1 = n_2 U_d$ (as well as $U_2 = n_2 U_p$). This brings us to the the equation of motion [Eq. (1)] used in the main text,

$$\ddot{x} + \omega_0^2[1 - \lambda\cos(2\omega t + \phi)]x + \Gamma\dot{x} + \alpha x^3 + \eta x^2\dot{x} = F_d\cos(\omega t + \theta), \tag{A3}$$

where $\alpha = \tilde{\alpha}/n_1^2$, $\eta = \tilde{\eta}/n_1^2$ and $F_d = U_d n_1 n_2/L$.

APPENDIX B: BASIC CHARACTERIZATION

In the following, we present the calibration measurements from which we obtained the numerical values of the coefficients for Eq. (A3).

Measuring the resonance frequency f_0 for varying dc tuning voltages U_{tune} allowed us to calculate C_1 as a function of the voltage applied across the diode. This is done with the formula

$$C_1 = \left[\omega_0^2 L - \frac{1}{C_2}\right]^{-1} \tag{B1}$$

with $\omega_0 = 2\pi f_0$ and with $L = 94\,\mu$H and $C_2 = 47$ nF the independently measured values of the coil inductance and of the second capacitance, respectively [Fig. 5(a)]. This calibration is also used to estimate the effect of the gate voltage U_{gate} that is applied to the opposite side of the diode. There, however, it is necessary to take into account the frequency-dependent

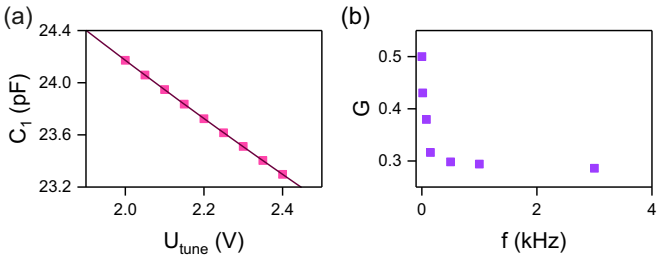

FIG. 5. (a) C_1 as a function of U_{tune} calculated from measurements of f_0 with Eq. (B1). (b) Frequency-dependent gain G of the voltage buffer used for U_{gate}. In the main text, we compensated for this frequency dependence.

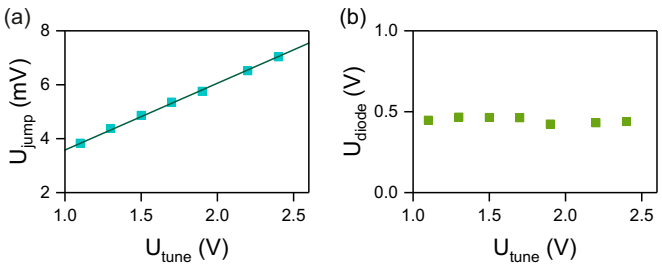

FIG. 7. (a) Maximum amplitude U_{jump} measured in parametric sweeps for different U_{tune}. (b) Extracted maximum voltage applied to the varactor diode before the jump.

gain characteristic of the operational amplifier that is used for U_{gate}. We calibrated the gain for different frequencies by measuring f_0 with a phase-locked loop while modulating U_{gate}, and by comparing the measured f_0 modulations with the value found for a dc tuning voltage U_{tune} [Fig. 5(a)]. In the measurements presented in the main paper, we compensated for the frequency-dependent gain by adapting the applied voltage such that the effective value of U_{gate} remained constant with frequency.

The quality factor Q was determined both from ringdown measurements and from a fit to the Lorentzian response of the resonator to small external driving. The two values were found to agree within the measurement precision. We obtained the ratio $F_d/U_d = 2.65 \times 10^{10}\,\text{s}^{-2}$ from a fit to the peak response amplitude U_{amp} with varying driving voltage amplitude U_d [Fig. 6(a)] using the formula

$$U_{\text{amp}} = \frac{F_d Q}{\omega_0^2}. \tag{B2}$$

Without external driving and with strong parametric pumping, the oscillator enters a region of parametric instability within a precisely defined frequency range, the so-called "Arnold tongue" [1]. The extent of this frequency range Δf as a function of U_p is shown in Fig. 6(b). Knowing that the threshold for parametric instability is $\lambda_{\text{th}} = 2/Q$, we fit the data with

$$\Delta f^2 = 2 f_0^2 \sqrt{\frac{\lambda^2}{4} - \frac{1}{Q^2}}, \tag{B3}$$

which yields U_{th}, i.e., the critical value of U_p above which parametric oscillations appear at resonance. From this, we

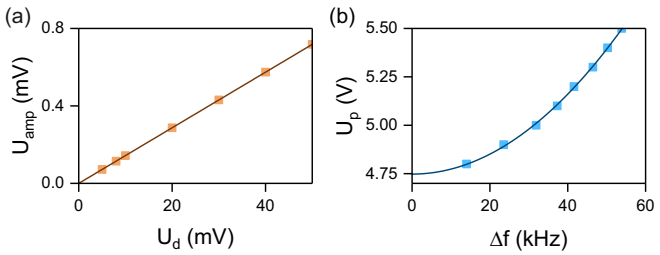

FIG. 6. (a) Peak amplitude U_{amp} of the Lorentzian response of the resonator measured in frequency sweeps with small driving voltage amplitudes U_d. (b) Width of the Arnold tongue Δf for varying parametric driving voltage amplitude U_p.

infer the relation between U_p and λ given in Eq. (2). The effective coefficient α of the Duffing nonlinearity was found from fitting the steady-state response of the parametron to the data in Fig. 1(d) [see Eq. (9) in Ref. [27]].

Finally, we investigated the origin of the termination of the large-amplitude branch in sweeps with parametric drive [see arrow in Fig. 1(d)]. In Fig. 7(a) we show the termination amplitude U_{jump}, i.e., the maximum amplitude before the branch is terminated, for sweeps with different tuning voltage U_{tune}. The linear dependency clearly points to the diode as the origin of the nonlinear damping term. When the oscillating voltage in the circuit becomes too large, it can cancel the reverse bias U_{tune} and make the diode conducting. During a short duration of the oscillation period, the diode then conducts electrical current, which leads to a loss of charge and, consequently, a breakdown of the parametric oscillation. Using the proportionality factor $\sim$0.0025 between U_{tune} and U_{jump}, we can determine the voltage across the varactor diode just before the jump [Fig. 7(b)]. This voltage is indeed close to the forward bias voltage expected for a silicon diode.

We found that we have to recalibrate η for different values of U_{tune} because of the changing reverse bias. By contrast, we neglect the relatively small changes due to U_{gate} for simplicity. It may be that some of the minor differences between measurement and simulations in Figs. 3 and 4 are due to this simplification.

APPENDIX C: SIMULATIONS

The dynamics of the oscillator subjected to gate voltage modulations was simulated by solving Eq. (A3) with $\omega_0 = \omega_0(t)$ and $\omega = \text{const} \approx \omega_0$. We follow Ref. [27] in rewriting the equation with dimensionless variables $\tau = \omega_0 t$ and $z = \sqrt{\alpha/(\omega_0^2)}x$, using a Van der Pol transformation to obtain slow-flow variables U and V, and performing the averaging over one period of a parametric pump cycle. This procedure yields two coupled first-order differential equations with variables $u = \bar{U}$ and $v = \bar{V}$:

$$\dot{u} = f_1(u, v) = -\frac{1}{2\Omega}\left\{\bar{\gamma}\Omega u + v\left[\sigma + \frac{\lambda}{2}\cos(\phi)\right] - u\frac{\lambda}{2}\sin(\phi) + \frac{3}{4}(u^2+v^2)v + \Omega\frac{\bar{\eta}}{4}(u^2+v^2)u - \bar{F}_0\sin(\theta)\right\}, \tag{C1}$$

$$\dot{v} = f_2(u, v)$$
$$= -\frac{1}{2\Omega}\left\{\bar{\gamma}\Omega v + u\left[-\sigma + \frac{\lambda}{2}\cos(\phi)\right] + v\frac{\lambda}{2}\sin(\phi) - \frac{3}{4}(u^2+v^2)u + \Omega\frac{\bar{\eta}}{4}(u^2+v^2)v + \bar{F}_0\cos(\theta)\right\}, \quad \text{(C2)}$$

where $\bar{\gamma} \equiv \gamma/(\omega_0)$, $\bar{\eta} \equiv \eta\omega_0/|\alpha|$, $\Omega \equiv \omega/\omega_0$, $\bar{F}_0 \equiv (F_0/\omega_0^3)\sqrt{|\alpha|}$, and $\sigma = 1 - \Omega^2$.

For a given $\omega_0(t)$, Eqs. (C1) and (C2) can be integrated numerically. We used the *itoint* function from the python package *sdeint*. The solutions in Fig. 3 were attained by using $\omega_0(t) = \omega_0(U_{\text{gate}} = 0) + \Delta\omega\cos(\omega_{\text{mod}}t)$.

APPENDIX D: LOGIC GATE OPERATIONS

The gate parametron can be used to implement logic operations as originally suggested Goto [17]. In his design, two parametrons P_1 and P_2 plus a "constant parametron" (e.g., a driving voltage U_ω) act on a parametron logic unit P_3. When the parametric drive of P_3 is switched off, the device becomes susceptible to the phase of the combined driving signals. The three driving sources perform a "majority vote" to determine the phase of P_3. When the parametric drive is switched on again, P_3 rings up to the corresponding phase state.

Logic operations with the gate parametron use a similar working principle [see Fig. 8(a)]. The component of the driving voltage at frequency f_d takes on the role of U_ω. In general, the coupling between gate parametrons should be chosen such that the driving produced by U_ω is equal to the effect of $P_{1,2}$. There are a few differences between ours and Goto's original design that we should comment on.

In our scheme, the parametric drive of $P_{1,2,3}$ is never switched off. Instead, a logic operation is performed by detuning P_3 from f_d for a defined amount of time, similar to half a modulation cycle in Fig. 2(c). This can be done with negative or positive gate voltages, for instance by ramping U_{gate} from 0 to 0.2 V and back. As shown in Figs. 8(b) and 8(c), the two signs cause the device to be detuned in opposite directions in frequency, which will cause different operations. The reason for the different outcomes is the hysteretic nature of the gate parametron or, in other words, the different phase response of the underlying harmonic resonator below and above its resonance frequency. In Fig. 8(d) we show the outcomes of different operations as a function of the phases of U_ω and $P_{1,2}$ (with "0" being defined as the phase of U_ω) and depending on the sign of U_{gate}. If an input of "1" is required from U_ω, the input signal must be inverted, either via a delay line or by inverse wiring as in Ref. [17].

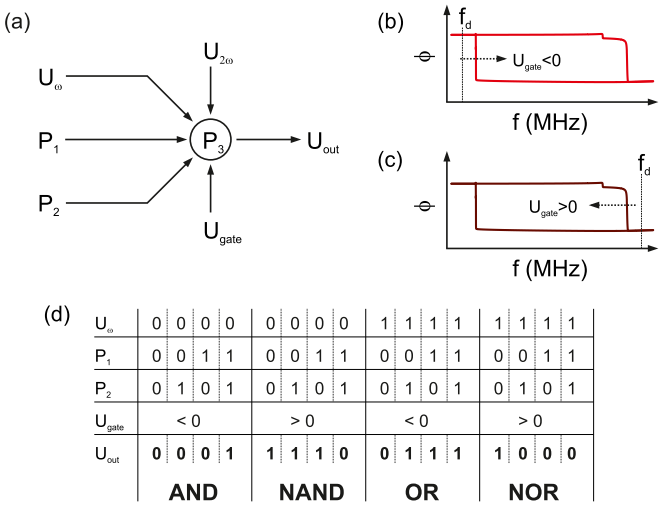

FIG. 8. (a) Schematic representation of a logic unit. P_1 and P_2 are two gate parametron devices that are acting on a third gate parametron, P_3. The two driving voltages at frequencies f_d and $2f_d = f_p$ are labeled U_ω and $U_{2\omega}$, respectively. Gate operations are achieved by applying voltage pulses via U_{gate}. The output of the logic operation is encoded in the phase of U_{out}. (b) Gate operations can be performed by applying a negative tuning voltage to U_{gate}, such that the device is effectively driven below its resonance frequency for a short time. The phase that is imprinted onto P_3 in this case is the (majority) phase of the combined drives U_ω, P_1, and P_2. Note that f_d is always constant. (c) For positive U_{gate}, the phase imprint is inverted and the phase that is imprinted onto P_3 is opposite to that of the combined drives. (d) Predicted outcome of logic operations. Here we have defined "0" as the phase of U_ω and "1" as the phase shifted by π.

Due to parametric symmetry breaking, the driving amplitudes of $P_{1,2}$ may vary slightly. This is not problematic as long as the difference is much smaller than the amplitudes themselves. A 2-to-1 majority voting has the same deterministic outcome as a 1.98-to-1.01 voting. For operations involving N sources, the amplitude difference should be much smaller than one Nth of each amplitude. For quantum operations, the amplitude difference might be more problematic than in the classical case.

In Goto's original design, each parametron was periodically switched on and off to allow information to travel through layers of devices [17]. This imposed a strict clocking of all devices and a rigid directionality for operations. The gate parametron allows operations without switching the parametric drive off. Gate voltage pulses applied to a single gate parametron can be used for state initialization as well as logic operations, allowing more versatile architectures and operations in different directions.

[1] M. C. Lifshitz and R. Cross, *Nonlinear Dynamics of Nanomechanical and Micromechanical Resonators* (Wiley-VCH, Weinheim, 2009), pp. 1–52.

[2] L. Kuzmin, K. Likharev, V. Migulin, and A. Zorin, IEEE Trans. Magnetics **19**, 618 (1983).

[3] B. Yurke, L. R. Corruccini, P. G. Kaminsky, L. W. Rupp, A. D. Smith, A. H. Silver, R. W. Simon, and E. A. Whittaker, Phys. Rev. A **39**, 2519 (1989).

[4] M. A. Castellanos-Beltran and K. W. Lehnert, Appl. Phys. Lett. **91**, 083509 (2007).

[5] C. Eichler and A. Wallraff, EPJ Quantum Tech. **1**, 2 (2014).
[6] A. Roy and M. Devoret, C. R. Phys. **17**, 740 (2016).
[7] D. Rugar and P. Grütter, Phys. Rev. Lett. **67**, 699 (1991).
[8] L. G. Villanueva, R. B. Karabalin, M. H. Matheny, E. Kenig, M. C. Cross, and M. L. Roukes, Nano Lett. **11**, 5054 (2011).
[9] J. Gieseler, B. Deutsch, R. Quidant, and L. Novotny, Phys. Rev. Lett. **109**, 103603 (2012).
[10] C. M. Caves, Phys. Rev. D **23**, 1693 (1981).
[11] R. E. Slusher, L. W. Hollberg, B. Yurke, J. C. Mertz, and J. F. Valley, Phys. Rev. Lett. **55**, 2409 (1985).
[12] G. Breitenbach, S. Schiller, and J. Mlynek, Nature (London) **387**, 471 (1997).
[13] T. Eberle, S. Steinlechner, J. Bauchrowitz, V. Händchen, H. Vahlbruch, M. Mehmet, H. Müller-Ebhardt, and R. Schnabel, Phys. Rev. Lett. **104**, 251102 (2010).
[14] I. Mahboob and H. Yamaguchi, Nat. Nanotechnol. **3**, 275 (2008).
[15] C. M. Wilson, T. Duty, M. Sandberg, F. Persson, V. Shumeiko, and P. Delsing, Phys. Rev. Lett. **105**, 233907 (2010).
[16] Z. Lin, K. Inomata, K. Koshino, W. D. Oliver, Y. Nakamura, J. S. Tsai, and T. Yamamoto, Nat. Commun. **5**, 4480 (2014).
[17] E. Goto, Proc. IRE **47**, 1304 (1959).
[18] S. Kirkpatrick, C. D. Gelatt, and M. P. Vecchi, Science **220**, 671 (1983).
[19] I. M. Georgescu, S. Ashhab, and F. Nori, Rev. Mod. Phys. **86**, 153 (2014).
[20] H. Goto, Sci. Rep. **6**, 21686 (2016).
[21] S. Puri, S. Boutin, and A. Blais, npj Quantum Inf. **3**, 18 (2017).
[22] A. Marandi, Z. Wang, K. Takata, R. L. Byer, and Y. Yamamoto, Nat. Photonics **8**, 937 (2014).
[23] I. Mahboob, H. Okamoto, and H. Yamaguchi, Sci. Adv. **2**, e1600236 (2016).
[24] T. Inagaki, K. Inaba, R. Hamerly, K. Inoue, Y. Yamamoto, and H. Takesue, Nat. Photonics **10**, 415 (2016).
[25] D. Ryvkine and M. I. Dykman, Phys. Rev. E **74**, 061118 (2006).
[26] Y. Kim, M.-S. Heo, G. Moon, J.-H. Kim, H.-R. Noh, and W. Jhe, Phys. Rev. A **82**, 063407 (2010).
[27] L. Papariello, O. Zilberberg, A. Eichler, and R. Chitra, Phys. Rev. E **94**, 022201 (2016).
[28] A. Leuch, L. Papariello, O. Zilberberg, C. L. Degen, R. Chitra, and A. Eichler, Phys. Rev. Lett. **117**, 214101 (2016).
[29] J. F. Rhoads and S. W. Shaw, Appl. Phys. Lett. **96**, 234101 (2010).
[30] I. Mahboob, C. Froitier, and H. Yamaguchi, Appl. Phys. Lett. **96**, 213103 (2010).
[31] A. Eichler, T. L. Heugel, A. Leuch, C. L. Degen, R. Chitra, and O. Zilberberg, Appl. Phys. Lett. **112**, 233105 (2018).
[32] Y. Zhang and M. I. Dykman, Phys. Rev. A **95**, 053841 (2017).
[33] T. L. Heugel, M. Biondi, O. Zilberberg, and R. Chitra, arXiv:1901.03232.